Constraining dark matter through 21-cm observations

Valdes, M.; Ferrara, A.; Mapelli, M.; Ripamonti, E.

Published in:
Monthly Notices of the Royal Astronomical Society

DOI:
10.1111/j.1365-2966.2007.11594.x

Publication date:
2007

Mon. Not. R. Astron. Soc. **377,** 245–252 (2007) doi:10.1111/j.1365-2966.2007.11594.x

Constraining dark matter through 21-cm observations

M. Valdés,[1]★ A. Ferrara,[1] M. Mapelli[1] and E. Ripamonti[2]

[1]*SISSA/ISAS, via Beirut 2-4, 34014 Trieste, Italy*
[2]*Kapteyn Astronomical Institute, University of Groningen, Postbus 800, 9700 AV, Groningen, The Netherlands*

Accepted 2007 February 4. Received 2007 January 5

ABSTRACT

Beyond reionization epoch cosmic hydrogen is neutral and can be directly observed through its 21-cm line signal. If dark matter (DM) decays or annihilates, the corresponding energy input affects the hydrogen kinetic temperature and ionized fraction, and contributes to the Lyα background. The changes induced by these processes on the 21-cm signal can then be used to constrain the proposed DM candidates, among which we select the three most popular ones: (i) 25-keV decaying sterile neutrinos, (ii) 10-MeV decaying light dark matter (LDM) and (iii) 10-MeV annihilating LDM. Although we find that the DM effects are considerably smaller than found by previous studies (due to a more physical description of the energy transfer from DM to the gas), we conclude that combined observations of the 21-cm background and of its gradient should be able to put constrains at least on LDM candidates. In fact, LDM decays (annihilations) induce differential brightness temperature variations with respect to the non-decaying/annihilating DM case up to $\Delta\delta T_{\rm b} = 8$ (22) mK at about 50 (15) MHz. In principle, this signal could be detected both by current single-dish radio telescopes and future facilities as Low Frequency Array; however, this assumes that ionospheric, interference and foreground issues can be properly taken care of.

Key words: intergalactic medium – cosmology: theory – dark matter – diffuse radiation.

1 INTRODUCTION

Cosmic recombination at $z \sim 1000$ left the gas in the Universe in a nearly uniform, dark, neutral state which we currently denote as the Dark Ages of the Universe. Gas remained neutral until the first luminous objects emerged at $z \sim 20$–30, leading to the complete reionization of the intergalactic medium (IGM) at a later, yet unknown, epoch.

The investigation of the Dark Ages is one of the frontiers of modern cosmology and a new generation of radio interferometers is currently in development to study the redshifted 21-cm hyperfine triplet–singlet level transition of the ground state of neutral hydrogen. Instruments such as the Low Frequency Array (LOFAR), the 21-Centimeter Array (21CMA), the Mileura Wide-Field Array (MWA) and the Square Kilometer Array (SKA), are expected to reach the sensitivity required to map the H I distribution at angular resolution of the order of a few arcmin (e.g. Peterson, Pen & Wu 2005; Kassim et al. 2004; Bowman, Morales & Hewitt 2006; Wyithe, Loeb & Barnes 2005).

The main scientific goal of such instruments is to perform an accurate tomography of matter during these remote cosmic epochs, and reconstruct in detail the latest phases of the reionization history. However, this might not be the only major achievement of such experiments. For example, an analysis of the features of H I 21-cm maps from the Dark Ages could also allow us to put constrains on the existence and nature of decaying and annihilating Dark Matter (DM). In fact, if DM actually decays or annihilates, the injection of high energy photons into the IGM would heat and ionize the neutral gas, leaving an imprint on the 21-cm background signal which could be directly observed (Furlanetto, Oh & Pierpaoli 2006b; Shchekinov & Vasiliev 2006).

The importance of DM decays and annihilations on the reionization history has been analysed in detail by several authors. Most authors have come to the conclusion that the effects of DM on the overall reionization process are relatively small and they cannot compete with those induced by more conventional ionizing sources as stars and (mini-) quasars. However, as we will explain in detail later on, radiation from decaying/annihilating DM might change the thermal and ionization history of the gas to such an extent that differences with the case in which DM is not considered are large enough to produce a clear signature in observable 21-cm signal. Assessing the amplitude of these deviations from the standard scenario requires a careful study of complex physical processes, and in particular of the amount of energy that can be transferred from the decay/annihilation products to the IGM. A recent study (Ripamonti, Mapelli & Ferrara 2007a, hereafter RMF07a) finds that only a relatively small fraction of the injected energy is effectively absorbed by the IGM and goes into heating and reionization. As a result, the effects on the 21-cm background signal might be smaller

★E-mail: valdes@sissa.it

than previously predicted (Furlanetto et al. 2006b; Shchekinov & Vasiliev 2006); hence, the question remains if the DM signal can still be observed by next generation radio interferometers. If so, this experiment would constitute a superb tool to distinguish among different DM candidates via their decaying/annihilating properties. In this paper, we calculate the effects of DM decays/annihilations on the 21-cm background for some of the most popular DM candidates, such as decaying or annihilating light dark matter (LDM) and decaying sterile neutrinos.

The rest of the paper is organized as follows. In Section 2, we briefly introduce the DM candidates and their effect on the IGM; in Section 3 we provide the basic equations to study the 21-cm radiation in the presence of decaying/annihilating DM. In Section 4, we present the results of our calculations, which are then discussed in Section 5. Throughout the paper we assume, in agreement with the 3-yr *Wilkinson Microwave Anisotropy Probe* data analysis (Spergel et al. 2006), a Lambda cold dark matter (ΛCDM) cosmology with $\Omega_{\rm m} = 0.24$, $\Omega_\Lambda = 0.76$, $h = 0.73$, $\Omega_{\rm b} = 0.042$, $H_0 = 100\,h\,{\rm km\,s^{-1}\,Mpc^{-1}}$.

2 BASIC PHYSICS

We are interested in calculating the effects on H I 21-cm line signal produced by two among the most popular low-mass DM candidates, i.e. LDM (∼1–10 MeV) and sterile neutrinos (∼2–50 keV). In the case of sterile neutrinos only the decay process is allowed; LDM particles instead can both decay and annihilate. We neglect heavier DM candidates (with mass larger than ∼100 MeV) because previous studies (Mapelli, Ferrara & Pierpaoli 2006) have already shown that even assuming that all the energy released following annihilations is immediately absorbed by the IGM, they represent a negligible heating/ionization source for the gas.

Both in the case of sterile neutrinos and of LDM, the rate of energy transfer per baryon to the IGM can be written as (RMF07a; Ripamonti, Mapelli & Ferrara 2007b, hereafter RMF07b)

$$\dot{E}_x(z) = f_{\rm abs}(z)\,\dot{n}_{\rm DM}(z)\,m_{\rm DM}\,c^2, \quad (1)$$

where $m_{\rm DM}$ is the mass of the DM particle and c is the speed of light. The energy absorbed fraction, $f_{\rm abs}(z)$, is discussed in detail in the following; $\dot{n}_{\rm DM}(z)$ is the decrease rate of the number of DM particles per baryon.

In the case of DM decays, $\dot{n}_{\rm DM}(z)$ is given by

$$\dot{n}_{\rm DM}(z) \simeq \frac{n_{\rm DM,0}}{\tau_{\rm DM}}, \quad (2)$$

where $n_{\rm DM,0}$ and $\tau_{\rm DM}$ are the current number of DM particles per baryon and the lifetime of DM particles, respectively.

For the annihilations,

$$\dot{n}_{\rm DM}(z) \simeq \frac{1}{2}\,n_{\rm DM,0}^2\,\mathcal{N}_{\rm b}(0)\,\langle\sigma\,v\rangle(1+z)^3, \quad (3)$$

where $\mathcal{N}_{\rm b}(0) = 2.5 \times 10^{-7}$ cm^{-3} is the current baryon number density (Spergel et al. 2006), and $\langle\sigma v\rangle$ is the thermally averaged DM annihilation cross-section. The values of $m_{\rm DM}$, $n_{\rm DM,0}$, $\tau_{\rm DM}$ and $\langle\sigma v\rangle$ depend from the properties of the chosen DM candidate (see Sections 2.1 and 2.3).

2.1 The energy absorbed fraction

The most delicate term in equation (1) is represented by $f_{\rm abs}(z)$, i.e. the fraction of the DM particle rest mass that is absorbed by the gas at a given redshift z; $f_{\rm abs}$ strongly depends on how the decay/annihilation products interact with the IGM. Since accounting for the physical processes which govern such interactions is quite complicated, most of previous studies assume that: (i) all the energy released by DM decays/annihilations is immediately absorbed (Hansen & Haiman 2004; Pierpaoli 2004; Biermann & Kusenko 2006; Mapelli et al. 2006), (ii) leave $f_{\rm abs}$ as a free parameter (Padmanabhan & Finkbeiner 2005; Zhang et al. 2006), or (iii) make a partial treatment of the energy redistribution (Chen & Kamionkowski 2004; Mapelli & Ferrara 2005).

Recently, RMF07a have calculated behaviour of $f_{\rm abs}(z)$ in detail, for the most common case in which the decay/annihilation products are photons, active neutrinos or electron–positron pairs. Photons are affected by Compton scattering and photoionization; for pairs, the relevant processes are inverse Compton scattering, collisional ionizations and positron annihilations.

RMF07a found that, if the decay/annihilation products are either photons and active neutrinos or pairs, $f_{\rm abs}$ is close to the maximum allowed value (equal to 0.5 for sterile neutrinos, due to the active neutrino production, and equal to 1 for LDM) only at very high redshift ($z \gg 100$). At lower redshifts, $f_{\rm abs}$ rapidly drops to values <0.1; also, the higher is the mass of the progenitor DM particle, the faster is the decrease of $f_{\rm abs}$. Thus, accounting for the correct $f_{\rm abs}(z)$ determination dramatically reduces the possible effects of DM decays and annihilations on the IGM heating and ionization (RMF07a) with respect to previous estimates.

In this paper, for the first time, we will adopt the correct estimate of $f_{\rm abs}(z)$ (as given in RMF07a) in order to evaluate the impact of DM decays and annihilations on 21-cm emission. Previous papers (e.g. Furlanetto et al. 2006b) have assumed a redshift-independent $f_{\rm abs}(z)$, which appears to be quite unrealistic (for a discussion, see Section 4) and leads to optimistic upper limits for the contribution of DM-related effects to 21-cm maps.

Differently from Furlanetto et al. (2006b), who do not select any specific DM candidate and leave the decay rate as a free parameter, we chose to consider three specific DM candidates (sterile neutrinos, decaying LDM and annihilating LDM). This choice allows us to give predictions which can be more easily related to other DM measurements, such as the X-ray constraints on the sterile neutrino mass (Boyarsky et al. 2006a; Boyarsky et al. 2006c; Watson et al. 2006) or the detection of the 511-keV emission line from the Galactic Centre (Knödlseder et al. 2005).

2.2 Sterile neutrinos

Many models of sterile neutrinos have been proposed, with mass ranging from eV to TeV. Here, we are interested in sterile neutrinos as warm DM (WDM) candidates, with masses of the order of a few keV (∼2–50 keV). These particles can decay into an active neutrino and a photon (Dolgov 2002, and references therein).

The mass (and thus the lifetime) of radiatively decaying sterile neutrinos can be constrained by the absence of any detection of X-ray lines consistent with photons due to sterile neutrino decays in galaxy clusters (Abazajian, Fuller & Tucker 2001; Abazajian 2006; Abazajian & Koushiappas 2006; Boyarsky et al. 2006b) or in galaxies (Watson et al. 2006 obtained the strongest constraints from the study of the Andromeda galaxy). Other constraints come from the comparison between the unresolved X-ray background and the expected contribution from sterile neutrino decays (Mapelli & Ferrara 2005; Boyarsky et al. 2006a).

In this paper, we consider the representative case of $m_\nu = 25$ keV sterile neutrinos, whose contribution to heating is maximum (RMF07a), due to the weakness of the available constraints on lifetime for neutrinos of such mass. For such particle, the upper

limits on the lifetime and the present number density number per baryon are $\tau_{\rm DM} = 9.67 \times 10^{25}$ s and $n_{\rm DM,0} = 1.88 \times 10^5$, respectively (see RMF07a, RMF07b). The contribution of other sterile neutrinos masses to the 21-cm line is expected to be comparable or smaller than for the case considered here.

2.3 Light dark matter

We define as LDM particles all the DM candidates whose mass is $1 \leqslant m_{\rm LDM}/{\rm MeV} \leqslant 100$. Such particles have been suggested as a possible source for the detected 511-keV excess from the Galactic Centre (Knödlseder et al. 2005). According to this scenario, their maximum allowed mass $m_{\rm LDM}$ should be 20 MeV, not to overproduce detectable gamma-rays via internal bremsstrahlung (Beacom, Bell & Bertone 2005), or even ∼3 MeV, if we consider also the production of gamma-rays for inflight annihilations of the positrons (Beacom & Yüksel 2006).

LDM can decay or annihilate, producing photons, neutrinos and pairs. We will treat both channels in detail and assume that the only decay/annihilation products are pairs, an assumption leading to an upper limit in terms of IGM heating (RMF07a).

We consider, as a template, the case of 10-MeV LDM particles, which again yields the most efficient heating case (see RMF07a). For such particles, the upper limits of the current number (per baryon), the lifetime and the cross-section are $n_{\rm DM,0} \sim 446$, $\tau_{\rm DM} = 4 \times 10^{25}$ s and $\langle \sigma v \rangle \sim 2.4 \times 10^{-28}$ cm^3 s^{-1}, respectively (RMF07a).

3 EFFECTS ON THE 21-CM RADIATION

3.1 Lyα pumping

The 21-cm line is associated with the hyperfine transition between the triplet and the singlet levels of the hydrogen ground state. This transition is governed by the spin temperature, $T_{\rm S}$, defined as

$$\frac{n_1}{n_0} = 3 \exp\left(-\frac{T_\star}{T_{\rm S}}\right), \tag{4}$$

where n_0 and n_1 are the number densities of hydrogen atoms in the singlet and triplet ground hyperfine levels, and $T_\star = 0.068$ K is the temperature corresponding to the transition energy.

In the presence of the cosmic microwave background (CMB) alone, the spin temperature reaches thermal equilibrium with $T_{\rm CMB} = 2.73(1+z)$ K on a short time-scale, making the H I undetectable in emission or absorption.

Two mechanisms can decouple $T_{\rm S}$ from $T_{\rm CMB}$: (i) collisions, which are effective mainly at $z \geqslant 70$ due to the higher mean IGM density, and (ii) scattering by Lyα photons – the so-called Wouthuysen–Field process or Lyα pumping (e.g. Wouthuysen 1952; Field 1959; Hirata 2006) – which couples $T_{\rm S}$ to the kinetic gas temperature $T_{\rm K}$ via the mixing of the hyperfine levels of the H I ground state through intermediate transitions to the excited 2p state.

The spin temperature is then given by the equation

$$T_{\rm S} = \frac{T_{\rm CMB} + y_\alpha T_{\rm k} + y_{\rm c} T_{\rm k}}{1 + y_\alpha + y_{\rm c}}, \tag{5}$$

where $T_{\rm k}$ is the kinetic temperature, and the Lyα and collisional coupling coefficients are given by the following expressions:

$$y_\alpha = \frac{P_{10} T_*}{A_{10} T_{\rm k}}, \tag{6}$$

$$y_{\rm c} = \frac{C_{10} T_*}{A_{10} T_{\rm k}}, \tag{7}$$

where

$$C_{10} = k_{10} n_{\rm H\,I} + n_{\rm e} \gamma_{\rm e}, \tag{8}$$

and

$$P_{10} = \frac{16}{27} \frac{\pi J_\alpha \sigma_\alpha}{h_{\rm p} \nu_\alpha}. \tag{9}$$

In the above equations, $A_{10} = 2.85 \times 10^{-15}$ s^{-1} is the spontaneous emission coefficient of the 21-cm line, P_{10} is the indirect de-excitation rate of the hyperfine structure levels. We write $P_{10} = 4P_\alpha/27$; in addition, $P_\alpha = (4\pi J_\alpha \sigma_\alpha)/(h_{\rm p}\nu_\alpha)$ is the outcome of the equation for the Lyα scattering rate,

$$P_\alpha = c \int {\rm d}\nu\, n(\nu) \frac{\sigma(\nu)}{\nu} = \frac{4\pi}{h} \int {\rm d}\nu\, \frac{J_\nu\, \sigma(\nu)}{\nu}, \tag{10}$$

in the case that $\sigma(\nu)$ is a δ function. A detailed investigation of the physics of the Wouthuysen–Field process (Hirata 2006) finds small corrections to these expressions which we neglect here for simplicity. The coefficient C_{10} in equation (8) is the collisional de-excitation rate by hydrogen atoms and electrons, where k_{10} is tabulated in Allison & Dalgarno (1969) for different temperatures; $\gamma_{\rm e}$, according to Liszt (2001), is

$$\log \gamma_{\rm e}(T_{\rm k}) = -9.607 + \log T_{\rm k}{}^{1/2} \exp\left[-(\log T_{\rm k})^{4.5}/1800\right], \tag{11}$$

for $T_{\rm k} \leqslant 10^4$ K, while $\gamma_{\rm e}(T_{\rm k} > 10^4\,{\rm K}) = \gamma_{\rm e}(T_{\rm k} = 10^4\,{\rm K})$.

For the Lyα pumping to be effective, a minimum Lyα background intensity, J_α, is required. This is given by the condition (Ciardi & Madau 2003)

$$J_\alpha \geqslant 9 \times 10^{-23}(1+z)\ {\rm erg\ cm^{-2}\ s^{-1}\ Hz^{-1}\ sr^{-1}}, \tag{12}$$

at the redshift of interest.

3.2 IGM evolution and 21-cm background

Next, we want to understand how DM decays/annihilations affect the thermal and ionization evolution of the IGM, which, in turn, determines the level of the 21-cm background signal. The equation that describes the evolution of the ionized fraction $x_{\rm e}$ is the following (see e.g. Chen & Miralda-Escudé 2004):

$$-\frac{{\rm d}x_{\rm e}}{{\rm d}z} = \frac{1}{H(z)(1+z)}[R_{\rm s}(z) - I_{\rm s}(z) - I_x(z)], \tag{13}$$

where $I_x = \dot{E}_x/E_0$ is the contribution to the ionization rate due to DM; $I_{\rm s}$ and $R_{\rm s}$ are the standard ionization and recombination rates per baryon. Considering equations (1)–(3), we have that

$$I_x = \chi_{\rm i}(z) \frac{\dot{E}_x}{E_0} = f_{\rm abs}(z) \chi_{\rm i}(z) \Gamma_x f_x \frac{m_{\rm p} c^2}{E_0} \tag{14}$$

for DM decays, and

$$I_x = \chi_{\rm i}(z) \frac{\dot{E}_x}{E_0} = f_{\rm abs}(z) \chi_{\rm i}(z) f_x \frac{m_{\rm p} c^2}{E_0} n_{\rm DM,0} \mathcal{N}_{\rm b}(z) \langle \sigma\ v \rangle \tag{15}$$

for DM annihilations. In the last two equations, $E_0 = 13.6$ eV is the hydrogen ionization threshold, $m_{\rm p}$ is the proton mass, $\chi_{\rm i}$ is the fraction of the energy absorbed by the IGM from DM decays/annihilations that goes into ionizations ($\chi_{\rm i} \sim (1 - x_{\rm e})/3$; see Shull 1979; Shull & van Steenberg 1985), $f_x = \Omega_x(z)/\Omega_{\rm b}(z)$, $\mathcal{N}_{\rm b}(z)$ is the baryon number density and $\Gamma_x = 1/\tau_{\rm DM}$.

The equation regulating the evolution of IGM temperature can be written as

$$(1+z)\frac{{\rm d}T_{\rm k}}{{\rm d}z} = 2T_{\rm k} + \frac{l_\gamma x_{\rm e}}{H(z)(1 + f_{\rm He} + x_{\rm e})}(T_{\rm k} - T_{\rm CMB}) - \frac{2\chi_{\rm h} \dot{E}_x}{3 k_{\rm b} H(z)(1 + f_{\rm He} + x_{\rm e})}, \tag{16}$$

where $l_\gamma = (8\sigma_T a_R T_{CMB}^4)/(3m_e c)$, χ_h is the fraction of the absorbed DM energy deposited into the IGM as heating (Shull & van Steenberg 1985) and $f_{He} = 0.24$ is the helium fraction by mass. The Lyα heating resulting from repeated scatterings as the photons are redshifted into the Lyman resonances is negligible as it has been recently shown (see e.g. Chen & Miralda-Escudé 2004). The ionization and temperature equations (13)–(16) are solved using a modified version of RECFAST (Seager, Sasselov & Scott 1999).

A third equation is needed in order to compute the 21-cm background: the one describing the evolution of the Lyα background intensity J_α. Following Madau, Meiksin & Rees (1997), we write

$$J_\alpha(z) = \frac{\mathcal{N}_H^2 hc}{4\pi H(z)} \left[x_e x_p \alpha_{2^2P}^{\rm eff} + x_e x_{H\,I} \gamma_{eH} + \frac{\chi_\alpha \dot{E}_x(z)}{\mathcal{N}_H h \nu_\alpha} \right], \qquad (17)$$

where the first two terms are the contributions from recombinations and collisional excitations by electron impacts, while the third term is the DM contribution.

In the last equation $\mathcal{N}_H = 0.92\mathcal{N}_b$ is the number density of hydrogen atoms, $\alpha_{2^2P}^{\rm eff}$ is the effective recombination coefficient to the 2^2P level (Pengelly 1964), which includes direct recombinations to the 2^2P level and recombinations to higher levels, followed by transitions to the 2^2P level via all possible cascade paths.

Finally, $\gamma_{eH} \approx 2.2 \times 10^{-8} \exp(-11.84/T_4)\,{\rm cm^3\,s^{-1}}$ is the collisional excitation rate of H I atoms photons by electron impacts; χ_α is the net fraction of the absorbed X-ray photons from DM decays/annihilations which is converted into Lyα photons (Shull & van Steenberg 1985), and $T_4 = T/(10^4\,{\rm K})$.

Once $T_S(z)$ has been determined through equation (5), we can obtain the 21-cm radiation intensity, which can be expressed by the differential brightness temperature between a neutral hydrogen patch and the CMB

$$\delta T_b \simeq \frac{T_S - T_{CMB}}{1+z}\,\tau, \qquad (18)$$

where τ is the optical depth of the neutral IGM at $21(1+z)$ cm

$$\tau \simeq \frac{3c^3 h_p A_{10}}{32\pi k_B \nu_0^2 T_S H(z)} \mathcal{N}_{H\,I}. \qquad (19)$$

In equation (19), h_p and k_B are the Planck and Boltzmann constants, respectively, $\nu_0 = 1420$ MHz is the 21-cm hyperfine transition frequency and $\mathcal{N}_{H\,I}$ is the local H I number density. If T_S is higher than T_{CMB}, the neutral IGM will be visible in emission against the CMB; on the contrary, if $T_S < T_{CMB}$ it will be visible in absorption.

4 RESULTS

In a Universe where DM does not decay or annihilate the spin temperature and the kinetic temperature of the gas track the CMB temperature down to $z \approx 300$, when the kinetic temperature starts to decrease adiabatically, $T_K \propto (1+z)^2$, while $T_{CMB} \propto (1+z)$. The collisions at this redshift are efficient at coupling T_S and T_K: the spin temperature subsequently tracks the kinetic temperature down to $z \sim 70$. At lower redshifts radiative coupling to the CMB becomes dominant and $T_S \to T_{CMB}$ again. As a result, for $30 \leqslant z \leqslant 300$ H I is visible in absorption against the CMB at wavelength of 21 $(1+z)$ cm. This scenario could change considerably if we allow for DM decay/annihilation, depressing or even erasing the absorption feature discussed above. Also, we note that different DM candidates leave different traces on the 21-cm background signal, and therefore it could be possible, in principle, to constrain directly the DM nature through 21-cm observations. To isolate the effect of DM, we will assume in the following that the entire cosmic DM content is constituted by particles of the considered type (sterile neutrinos or LDM), i.e. $\Omega_X = \Omega_m - \Omega_b$.

4.1 WDM: 25-keV sterile neutrino decay

In Fig. 1, we compare the effects of 25-keV sterile neutrino decays on T_S assuming either the physically motivated value of f_{abs} (left-hand panel) or the commonly adopted value $f_{abs} = 0.5$ (right-hand panel), i.e. the maximum allowed value for sterile neutrinos corresponding to complete absorption. In addition, in each of the panels we explore the differences between models with or without the energy injection term due to DM decays. We will refer in the following to the latter as the *standard* case, for brevity.

With respect to the case without DM energy injection, we find, independently of the assumption made for f_{abs}, a higher kinetic temperature and hydrogen ionization fraction. However, such an enhancement produces only very modest T_S differences with respect to the standard case, which has some effect on the differential brightness temperature δT_b. The difference $T_S - T_{CMB}$ remains extremely small due to the limited ability of the Lyα pumping to decouple the two temperatures.

The main difference between the results obtained from the two f_{abs} assumptions is the behaviour of T_K at $z \sim 10$–70. When we use the realistic f_{abs} value, the IGM kinetic temperature positively deviates at

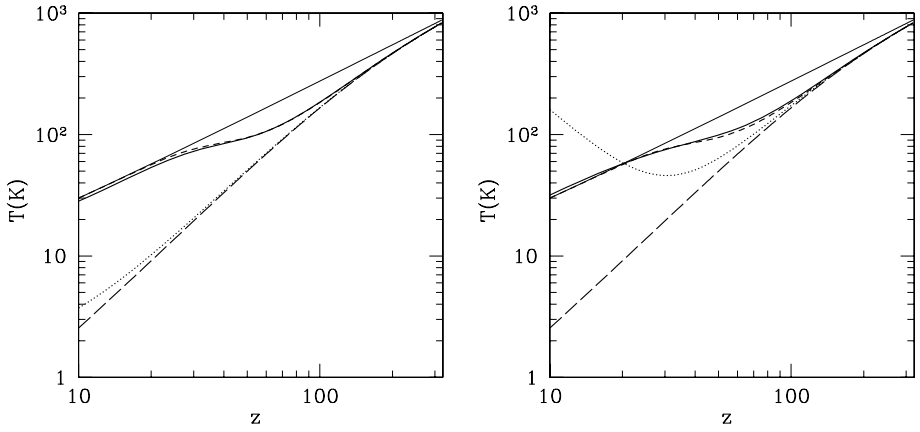

Figure 1. Left-hand panel: T_S and T_k as a function of redshift (25-keV sterile neutrino decays, f_{abs} as in RMF07a). Thin solid line: T_{CMB}; thick solid (short dashed) line: T_S with (without) 25-keV neutrino decays; dotted (long dashed) line: T_k with (without) 25-keV neutrino decays. Right-hand panel: T_S and T_k as a function of redshift for 25-keV sterile neutrino decays and for $f_{abs} = 0.5$. The lines are the same as in the left-hand panel.

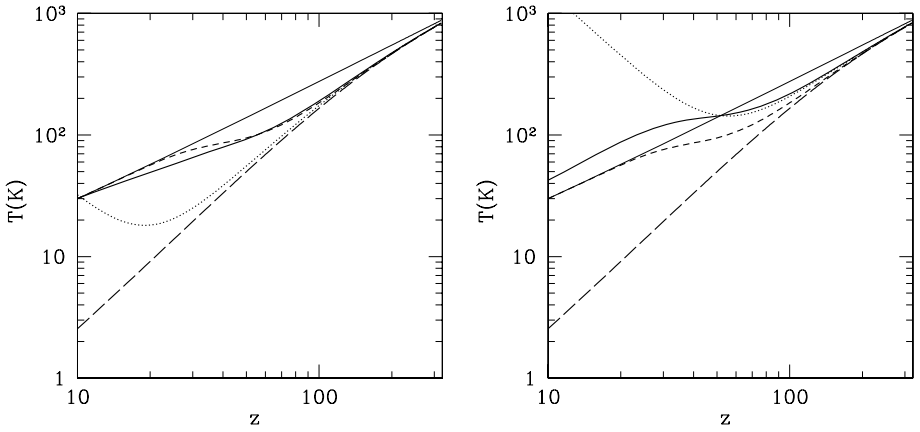

Figure 2. Left-hand panel: T_S and T_k as a function of redshift (10-MeV LDM decays, f_{abs} as in RMF07a). Thin solid line: T_{CMB}; thick solid (short dashed) line: T_S with (without) 10-MeV LDM decays; dotted (long dashed) line: T_k with (without) 10-MeV LDM decays. Right-hand panel: T_S and T_k as a function of redshift for 10-MeV LDM decays and for $f_{abs} = 1$. The lines are the same as in the left-hand panel.

most by 50 per cent from its standard evolution; if instead $f_{abs} = 0.5$ is adopted (e.g. as assumed for example by Furlanetto et al. 2006b), the kinetic temperature overshoots the CMB one and reaches very large values (>100 K) at low redshifts.

4.2 LDM: 10-MeV decay/annihilation

We now turn to the analysis of LDM candidates. Following the same procedure as in the previous section, we compare the results of the two different assumptions for f_{abs} (note that for LDM, the constant absorbed fraction case corresponds to $f_{abs} = 1$, see Section 2.1), and also test the effects of decays/annihilation against the standard case.

We start from the analysis of the realistic f_{abs} case (Fig. 2, left-hand panel) for decaying LDM. The most striking feature is that the evolution of T_K decouples from the adiabatic one already at $z \approx 50$, and starts to increase below $z \approx 20$, reaching $T_K = 30$ K at $z = 10$. Such thermal history forces T_S to remain below T_{CMB} for a much longer redshift interval (down to $z = 10$) than in the standard case, in which $T_S \approx T_{CMB}$ already at $z \approx 25$. Interestingly, this effect extends the frequency range in which the IGM can be observed in absorption to higher values. The main physical reason for the larger impact of LDM decays on T_S with respect to sterile neutrinos analysed above basically lies in the larger f_{abs} value (approximately a factor of 10 below $z = 30$) of LDM particles; this is on top of their larger rest mass. The higher heating rate increases both T_K and the Lyα background (i.e. y_α), thus pushing T_S away from T_{CMB}.

When f_{abs} is instead artificially forced to be constant and equal to unity (Fig. 2, right-hand panel), the physical arguments given above can still be used to interpret the results, but the deviation from the standard case is much more dramatic, and results in an overestimate of the LDM decays impact. For example, T_K becomes larger than T_{CMB} already at $z \approx 50$ and stays above it thereafter, reaching >1000 K at $z = 10$. The increase is so strong that it essentially erases the absorption feature expected in the standard case above $z = 30$. The IGM according to this prescription should be observed in emission up to very high redshifts.

For comparison sake, we note that this case has nearly the same decay rate, $\Gamma_X = 2.5 \times 10^{-26}\ s^{-1}$, as that assumed in one of the cases explored by Furlanetto et al. (2006b) (dot–dashed line in fig. 1 of that paper). Consistently, the evolution of T_K from the two studies is essentially the same.

Finally, we turn to the case of annihilating LDM (Fig. 3). As usual, the left-hand panel of that figure reports the case in which the realistic, redshift dependent, values of f_{abs} are assumed. In this case, the kinetic temperature deviates from the standard adiabatic evolution at extremely high redshifts ($z > 200$): this is because the

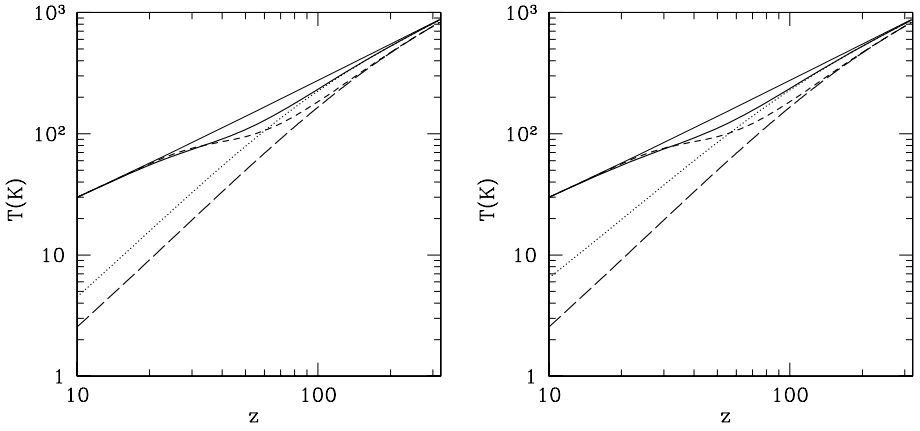

Figure 3. Left-hand panel: T_S and T_k as a function of redshift (10-MeV LDM annihilations, f_{abs} as in RMF07a). Thin solid line: T_{CMB}; thick solid (short dashed) line: T_S with (without) 10-MeV LDM annihilations; dotted (long dashed) line: T_k with (without) LDM annihilations. Right-hand panel: T_S and T_k as a function of redshift for 10-MeV LDM annihilations and for $f_{abs} = 1$. The lines are the same as in the left-hand panel.

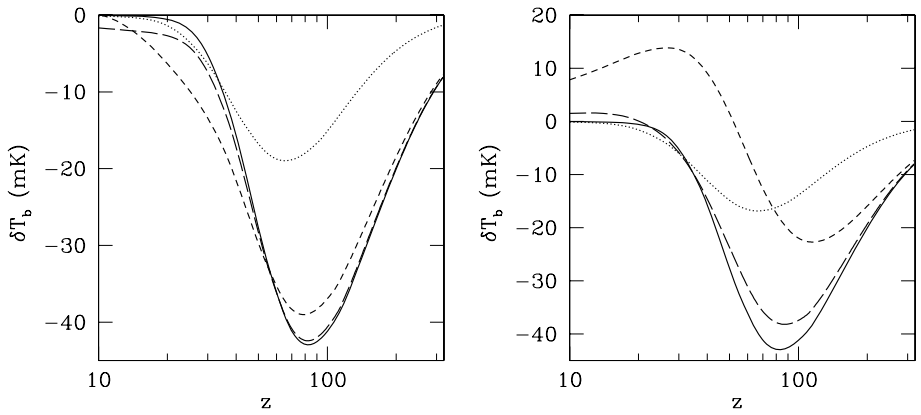

Figure 4. Left-hand panel: 21-cm differential brightness temperature as a function of redshift. The solid line shows $\delta T_{\rm b}$ without decaying/annihilating DM, while the long dashed, short dashed and dotted lines refer to $\delta T_{\rm b}$ with 25-keV decaying WDM, 10-MeV decaying LDM and 10-MeV annihilating LDM, respectively. Calculations were performed assuming $f_{\rm abs}$ as in RMF07a. Right-hand panel: 21-cm differential brightness temperature as a function of redshift as in the left-hand panel. Calculations were performed assuming $f_{\rm abs} = 0.5$ for sterile neutrinos and $f_{\rm abs} = 1$ in the other cases.

annihilation process depends on the square of the baryon density. As a result, its contribution predominantly occurs at early epochs and progressively vanishes with time, as realized also from the fact that below $z = 100$ the $T_{\rm K}$ curve is simply shifted to a higher adiabat. This fact causes the spin temperature to remain closer to (although always lower than) $T_{\rm CMB}$, thus preserving the standard absorption feature. Quite remarkably the results assuming the realistic $f_{\rm abs}$ values do not differ appreciably from those obtained by imposing $f_{\rm abs} = 1$ (Fig. 3, right-hand panel). As pointed out before, the effects of annihilating DM are evident only at very high redshift, where the detailed calculation gives $f_{\rm abs} \approx 1$ (see RFM06a), thus making the non-evolving $f_{\rm abs}$ approximation acceptable.

4.3 Global 21-cm background

Having obtained the evolution of $T_{\rm S}$ for the different DM candidates, we are now ready to compute for each case the quantity that is most readily associated with observations, i.e. the differential brightness temperature, $\delta T_{\rm b}$. These are shown in Fig. 4 for the realistic (left-hand panel) and the constant $f_{\rm abs}$ (right-hand panel) cases, respectively. In addition, to facilitate the comparison, we have also plotted in Fig. 5 the brightness temperature deviation $\delta T_{\rm b} - \delta T_{\rm b,0}$ of the various models from the standard one, restricted to the realistic $f_{\rm abs}$ evolution only.

As usual, we start our analysis from the realistic $f_{\rm abs}$ case. For sterile neutrinos (long dashed curves), the characteristic absorption feature in the 21-cm background signal expected at $30 \leqslant z \leqslant 300$ is only slightly modified from the standard case (solid line): the maximum difference is found to be only ≈ -2 mK in the range $z \sim 10$–40. Yet, such a small signature of WDM decays could still be in principle observable: even modest sized single-dish radio telescopes can reach the required mK sensitivity in an all-sky observation. The real challenge for the observation is represented by the ability to disentangle this cosmological signal from the various foregrounds (particularly the Galactic synchrotron emission) which could be several orders of magnitude brighter. The case of decaying 10-MeV LDM (short dashed lines in Fig. 4) is more interesting, as the difference with the standard case is larger. For this case, we find that the deviation is predicted to be $\approx -(5$–$8)$ mK in the range $20 < z < 40$. Such an amplitude could be detected by LOFAR or SKA after a 1000-h all-sky integration and by most single-dish radio telescopes, provided foreground contamination is taken care of. Finally, when LDM annihilations are considered, a considerably different $\delta T_{\rm b}$ evolution is obtained with respect to the standard case. Larger deviations are present in the entire range $40 < z < 200$, where the energy input of LDM annihilations forces $\delta T_{\rm b}$ to values larger than -20 mK, about two times smaller (in absolute value) than for the standard evolution. Such a large difference could in principle facilitate discriminating the annihilation scenario from the standard one. In practice, though, foregrounds and ionospheric contamination become more severe at the low observing frequencies implied by these high redshifts.

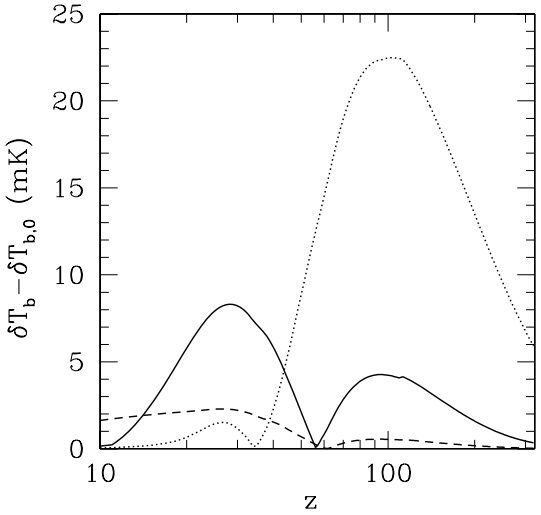

Figure 5. 21-cm differential brightness temperature difference in mK between the three DM cases considered and a non-decaying–annihilating DM scenario. The dashed, solid and dotted lines correspond to 25-kev sterile neutrino decays, 10-Mev LDM decays and 10-MeV annihilations case, respectively.

Although of academic interest only, it is instructive to compare the constant $f_{\rm abs}$ cases (Fig. 4, right-hand panel) with the previous results. As seen clearly form the figure, considerably different conclusions would be drawn. First, sterile neutrino would drive $\delta T_{\rm b}$ to positive values, resulting in an emission signal below $z = 20$; a similar trend is also obtained for LDM decays, whose effects are seen in 21-cm emission with an amplitude of about 10 mK. The results for LDM

annihilation instead do not show appreciable dependences on the $f_{\rm abs}$ prescription, for the reasons discussed above.

5 DISCUSSION

From the results obtained in this paper, we conclude that it is in principle possible to observe the H I 21-cm signal from the Dark Ages produced by the energy input due to decays/annihilations of the most popular light/warm DM candidates. If so, radio observations might represent one of the most promising tools to study the nature of DM, as different particles are predicted to leave a specific signature on the signal. The sensitivity required to measure the 21-cm background signal can be achieved not only by the next generation of radio interferometers but also by existing radio observatories.

However, the various foregrounds (i.e. Galactic free–free and synchrotron emission, unresolved extragalactic radio sources, free–free emission from ionizing sources, synchrotron emission from cluster radio haloes and relics) are much stronger than the cosmological signal, and will certainly prove extremely difficult to remove. Hence, a clear detection could be challenging to achieve.

It is beyond the scope of this paper to deal in detail with the problems of ionospheric scintillation and foreground contamination. A number of studies have discussed the foregrounds complications in some detail (e.g. Shaver et al. 1999; Oh & Mack 2003; Di Matteo, Ciardi & Miniati 2004), and we refer the reader to those papers for more information. For our aims it is sufficient to say that in general the sky temperature can be roughly described as

$$T_{\rm sky} \sim 180 \left(\frac{\nu}{180\ {\rm MHz}} \right)^{-2.6} {\rm K} \qquad (20)$$

(see e.g. Furlanetto, Oh & Briggs 2006a) and is, at the frequencies of interest, several orders of magnitude higher than the cosmological 21-cm background signal.

The success of the 21-cm background observations to constrain DM will depend on the capability of effectively removing the foregrounds and of correcting for ionospheric variations (e.g. Gnedin & Shaver 2004; Zaldarriaga, Furlanetto & Hernquist 2004; Morales, Bowman & Hewitt 2006; Santos, Cooray & Knox 2005).

An alternative method to study the 21-cm backgrounds is by separating its spectral features from the smooth foreground spectrum (e.g. Furlanetto 2006; Shaver et al. 1999). Fig. 6 shows the gradient of $\delta T_{\rm b}$ for the DM candidates studied here. It is clear from the figure that the gradients are higher and easier to constrain in the frequency range $\nu = 1420/(1+z)$ MHz $\sim$ 10–40 MHz. The foreground gradients, however, increase with decreasing frequency making it difficult to predict the best frequencies to get to for a successful detection.

Discriminating among different DM cases would imply the ability to distinguish the difference in brightness temperature and/or in its gradient with respect to the standard scenario. We define these two quantities as $\Delta\delta T_{\rm b} = \delta T_{\rm b} - \delta T_{\rm b}{}^{0}$ and $\Delta\delta T_{\rm b}/\Delta\nu = {\rm d}\delta T_{\rm b}/{\rm d}\nu - {\rm d}\delta T_{\rm b}{}^{0}/{\rm d}\nu$, where the 0 stands for the standard (i.e. non-decaying/annihilating) DM scenario.

Fig. 7 shows $\Delta\delta T_{\rm b}$ versus $\Delta\delta T_{\rm b}/\Delta\nu$ for the three DM models: the blue triangles correspond to 10-MeV annihilations, the red squares to 10-MeV decays and the black stars to the 25-keV sterile neutrino decays. The points are separated by 1-MHz steps in a range that goes from 5 to 130 MHz. As the sensitivity is somewhat uncertain for the different proposed 21-cm experiments, we assume as a guideline that a successful detection requires $\Delta\delta T_{\rm b} > 3$ mK and $\Delta\delta T_{\rm b}/\Delta\nu > 0.6$ mK MHz^{-1}, respectively. The adopted value for $\Delta\delta T_{\rm b}$ is a conservative one given that mK sensitivities are already achievable in all-sky observations even by existing single-dish radio telescopes. It has been chosen so to partially take into consideration the difficulties associated with foregrounds removal.

The shaded area covers the parameter space corresponding to likely non-detections. For the 25-keV sterile neutrinos case the points lie almost entirely within the shaded area, thus future observations would hardly be able to pin down this scenario.

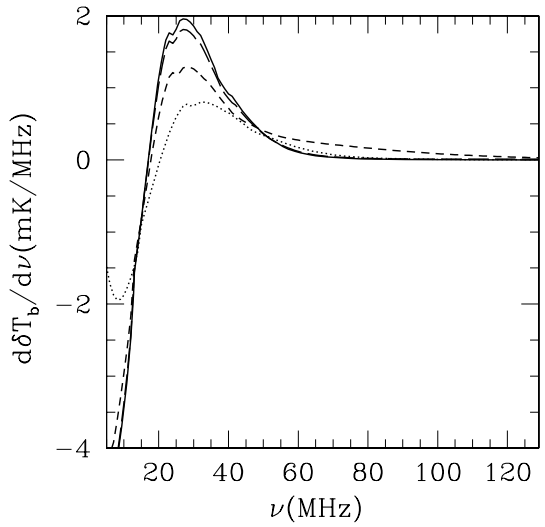

Figure 6. Gradient of the 21-cm differential brightness temperature. The solid line shows $\mathrm{d}\delta T_{\rm b}/\mathrm{d}\nu$ without decaying/annihilating DM; while the long dashed, short dashed and dotted lines refer to $\mathrm{d}\delta T_{\rm b}/\mathrm{d}\nu$ with 25-keV decaying WDM, 10-MeV decaying LDM and 10-MeV annihilating LDM, respectively. Calculations were performed assuming $f_{\rm abs}$ as in RMF07a.

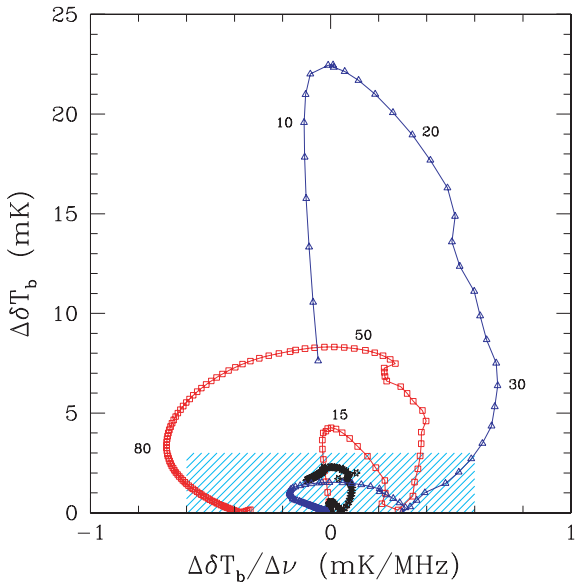

Figure 7. Deviations of the differential brightness temperature (y-axis) and its gradient (x-axis) from those predicted in the standard case. The diagram illustrates the capability of constraining DM with future 21-cm observations. The black stars, red squares and blue triangles represent 25-keV decaying WDM, 10-MeV decaying LDM and 10-MeV annihilating LDM, respectively. The shaded area indicates the parameter space in which detection is excluded given the expected observational capabilities. Numbers along the curves refer to frequencies in MHz units.

In the case of decaying or annihilating 10-MeV LDM, positive detections could be achieved on different frequency ranges. For the decays the ideal frequencies to study would be 40–80 MHz, where $\Delta\delta T_{\rm b} \gtrsim 4$ mK, and 80–90 MHz, where $\Delta\delta T_{\rm b} \sim 2$ mK but $\Delta\delta T_{\rm b}/\Delta\nu \gtrsim 0.6$ mK MHz^{-1}. At $\nu \geqslant 90$ MHz, or $z \leqslant 15$, the first luminous sources start having a dominant impact on the IGM and the small modifications from decaying/annihilating DM would not be visible.

For the 10-MeV LDM annihilations case, the best observing frequencies seem to be 10–30 MHz. At these frequencies $\Delta\delta T_{\rm b} \gtrsim 6$ mK with a peak of over 20 mK at 10–20 MHz. Observations at such low frequencies are particularly difficult and probably future radio interferometers will not reach such large wavelengths. Probably 30 MHz is the minimum frequency which will be achieved by next generation instruments, and the frequency at which it will then be possible to constrain 10-MeV annihilating LDM.

We conclude then that it is likely that future observations of the 21-cm background radiation will allow us to effectively constrain among some of the DM candidates, which by decays or annihilations can influence deeply the properties of the IGM.

Nevertheless our study shows that accounting for the physical evolution of $f_{\rm abs}(z)$ strongly reduces the amplitude of DM effects on the IGM with respect to those predicted by previous studies: for example we find that the effect of 25-keV decaying sterile neutrinos would be hardly observable.

REFERENCES

Abazajian K., 2006, Phys. Rev. D, 73f, 3506
Abazajian K., Koushiappas S. M., 2006, Phys. Rev. D, 74, 023527
Abazajian K., Fuller G. M., Tucker W. H., 2001, ApJ, 562, 593
Allison A. C., Dalgarno A., 1969, ApJ, 158, 423
Beacom J. F., Yüksel H., 2006, Phys. Rev. Lett., 97g, 1102
Beacom J. F., Bell N. F., Bertone G., 2005, Phys. Rev. Lett., 94q, 1301
Biermann P. L., Kusenko A., 2006, Phys. Rev. Lett., 96, 1301
Bowman J., Morales M., Hewitt J., 2006, ApJ, 638, 20
Boyarsky A., Neronov A., Ruchayskiy O., Shaposhnikov M., 2006a, MNRAS, 370, 213
Boyarsky A., Neronov A., Ruchayskiy O., Shaposhnikov M., 2006b, Phys. Rev. D, 74, 103506
Boyarsky A., Neronov A., Ruchayskiy O., Shaposhnikov M., Tkachev I., 2006c, preprint (astro-ph/0603660)
Chen X., Kamionkowski M., 2004, Phys. Rev. D, 70, 043502
Chen X., Miralda-Escudé J., 2004, ApJ, 602, 1
Ciardi B., Madau P., 2003, ApJ, 596, 1
Di Matteo T., Ciardi B., Miniati F., 2004, MNRAS, 355, 1053
Dolgov A. D., 2002, Phys. Rep., 370, 333
Field G. B., 1959, ApJ, 129, 551
Furlanetto S. R., 2006, MNRAS, 371, 867
Furlanetto S. R., Oh S. P., Briggs F. H., 2006a, Phys. Rev., 433, 181
Furlanetto S. R., Oh S. P., Pierpaoli E., 2006b, Phys. Rev. D, 74j, 3502
Gnedin N. Y., Shaver P. A., 2004, ApJ, 608, 611
Hansen S. H., Haiman Z., 2004, ApJ, 600, 26
Hirata C. M., 2006, MNRAS, 367, 259
Kassim N. E., Lazio T. J. W., Ray P. S., Crane P. C., Hicks B. C., Stewart K. P., Cohen A. S., Lane W. M., 2004, Planet. Space Sci., 52, 1343
Knödlseder J. et al., 2005, A&A, 441, 513
Liszt H., 2001, A&A, 371, 698
Madau P., Meiksin A., Rees M. J., 1997, ApJ, 475, 492
Mapelli M., Ferrara A., 2005, MNRAS, 364, 2
Mapelli M., Ferrara A., Pierpaoli E., 2006, MNRAS, 369, 1719
Morales M. F., Bowman J. D., Hewitt J. N., 2006, ApJ, 648, 767
Oh S. P., Mack K. J., 2003, MNRAS, 346, 871
Padmanabhan N., Finkbeiner D. P., 2005, Phys. Rev. D, 72b, 3508
Pengelly R. M., 1964, MNRAS, 127, 145
Peterson J. B., Pen U. L., Wu X. P., 2005, in Kassim N. E., Pérez M. R., Junor W., Henning P. A., eds, ASP Conf. Ser. Vol. 345, Searching for Early Ionization with the Primeval Structure Telescope. Astron. Soc. Pac., San Francisco, p. 441
Pierpaoli E., 2004, Phys. Rev. Lett., 92, 031301
Ripamonti E., Mapelli M., Ferrara A., 2007a, MNRAS, 374, 1067 (RMF07a)
Ripamonti E., Mapelli M., Ferrara A., 2007b, MNRAS, 375, 1399 (RMF07b)
Santos M. G., Cooray A., Knox L., 2005, ApJ, 625, 575
Seager S., Sasselov D. D., Scott D., 1999, ApJ, 523, 1
Shaver P., Windhorst R., Madau P., de Bruyn G., 1999, A&A, 345, 380
Shchekinov Y. A., Vasiliev E. O., 2006, MNRAS submitted (astro-ph/0604231)
Shull J. M., 1979, ApJ, 234, 761
Shull J. M., van Steenberg M. E., 1985, ApJ, 298, 268
Spergel D. N. et al. 2006, ApJ, submitted
Watson C. R., Beacom J. F., Yüksel H., Walker T. P., 2006, Phys. Rev. D, 74c, 3009
Wouthuysen S. A., 1952, AJ, 57, 31
Wyithe J. S., Loeb A., Barnes D., 2005, ApJ, 634, 715
Zaldarriaga M., Furlanetto S. R., Hernquist L., 2004, ApJ, 608, 622
Zhang L., Chen X., Lei Y.-A., Si Z., 2006, Phys. Rev. D, 74, 103519

This paper has been typeset from a TEX/LATEX file prepared by the author.